A study on the application of two different acoustic analogies to experimental PIV data

V. Koschatzky,[a] J. Westerweel, and B. J. Boersma
Laboratory for Aero and Hydrodynamics, Delft University of Technology, Mekelweg 2-Delft, Zuid-Holland 2628 CD, The Netherlands

(Received 15 December 2010; accepted 4 May 2011; published online 24 June 2011; publisher error corrected 30 June 2011)

The aim of the present study is to compare two different acoustic analogies applied to time-resolved particle image velocimetry (PIV) data for the prediction of the acoustic far-field generated by the flow over a rectangular cavity. We consider the model problem of sound radiating from an open, two-dimensional, shallow cavity with an aspect ratio of 2 at a Reynolds number of 3.0×10^4 (based on the cavity length). The study is carried out by simultaneous high-speed two-dimensional PIV and sound measurements. The instantaneous flow field is obtained from the PIV measurements. The emitted sound is then calculated using Curle's analogy and Vortex Sound Theory. To our knowledge, Vortex Sound Theory is used here for the first time in combination with time-resolved PIV data. The acoustic analogies are derived through rather different pathways, and the mathematical schemes used to solve the equations are sensitive in a different way to factors such as data resolution, noise level, and complexity of the geometry. Both methods indicate that the trailing edge of the cavity is the main sound source. The predictions of the acoustic field obtained by applying the two methods are analyzed and compared with the measured sound. For the presented case, the results show that both analogies estimate the overall sound pressure level quite well and that they give very similar results, both in total intensity and in the spectral distribution of the emitted sound. © *2011 American Institute of Physics*. [doi:10.1063/1.3596730]

I. INTRODUCTION

Contemporary investigation of aeroacoustics is performed by using both experimental and numerical studies. The problem is rather complex: it usually involves multiple physical processes; the governing equations are non linear; there is a wide range of length scales to be considered because of the separation between the flow and the acoustic scales; high Reynolds and Mach numbers are often involved; and the flow might occur in the proximity of solid surfaces which are frequently geometrically complex. All the methods that have been developed are useful in providing important insight into some specific aspects, but a general and exhaustive technique able to solve various acoustic problems is not yet available. It is therefore important to work on the development of new techniques that can help in the study of those problems that are difficult to approach with the established methods. It is in this spirit, with the intention to cover some of the open gaps, that the proposed methods are investigated.

Traditional experimental investigation follows different approaches. In industry, where the main focus is the localization of the sound sources rather than the study of the physical mechanisms of sound production, the main role is played by surface pressure sensors and microphone measurements. The most common use of microphones is beamforming (see Dougherty[1] for an overview of the method and the work of Brooks and Humphreys[2] for recent improvements): this is a technique where the microphones are organized in large arrays positioned in the acoustic far field. The phase shift in the microphone signals permits to reconstruct the locations where sound originates. Beamforming is a simple and rapid measurement technique, which is able to locate the sound sources and to follow their temporal evolution, but cannot provide any information about the nature of the sound source. In order to obtain this kind of information, the microphone measurements in the propagation region are usually performed in combination with flow measurements in the source region (by means of laser doppler anemometry (LDA), hot wire anemometry (HWA), and particle image velocimetry (PIV)), for two points space-time correlation studies (see the work of Henning *et al.*[3,4] for some recent results). Those studies can provide useful information, their limitation lies in the need of anechoic facilities to be properly performed and on the choice of the flow quantity to be used for the correlation that is not always well related with the actual acoustic source. Computational studies for the investigation of flow-generated sound follow two main approaches (see Wang *et al.*[5] and Colonius and Lele[6] for a complete review and analysis): a direct approach and an indirect, or hybrid, approach. In the direct approach, the sound is computed together with its fluid dynamic source field by solving the compressible flow equations (for instance by direct numerical simulation (DNS) or large eddy simulation (LES)). This method avoids any modeling approximations of

[a]Author to whom correspondence should be addressed. http: //dutw1479.wbmt.tudelft.nl/~valentina. Electronic mail: v.koschatzky@tudelft.nl.

the radiated sound and, therefore, the solution is as close as possible to the physical solution once the problem is well posed in terms of resolution and boundary conditions, aspects that are usually quite critical.[5,7] Because of the absence of modeling, the direct computation approach by DNS is essential for the generation of databases for developing and evaluating sound prediction models. However, its high computational cost limits its use to simple flow configurations at low or moderate Reynolds numbers. In a hybrid approach, the computation of the flow is decoupled from the computation of the sound, which can be done in a post-processing step based on an aeroacoustic theory (i.e. via integral methods, also known as acoustic analogies, or by numerical methods such as the linearized propagation equations). The advantage is that the most appropriate method can be chosen for each of the two steps, lowering the computational cost and, hence, broadening the possible applications. On the other hand, this approach is based on the fundamental assumption of the separation between the flow and the acoustic scales.

Recent and fast developments in laser and camera technology have opened the way to new measurement approaches for aeroacoustics that make it possible to use velocity data fields, obtained from time-resolved experimental PIV measurements, in the evaluation of acoustic sources. This new methodology provides insight in the sound sources that was previously not possible to achieve with the established experimental methods. It also permits the experimental investigation in those situations where other measurements would not be possible, for example, in the presence of a noisy environment or when a suitable anechoic tests facility is unavailable. In addition, it allows the estimation of the acoustic emission, coupled to the proper acoustic model, in the same fashion as done in hybrid computational approaches. Compared to computational studies, the methods proposed here have both advantages and disadvantages. The temporal and spatial resolutions achievable by PIV, as well as the size of the investigated domain, are currently still considerably modest in comparison to what can be achieved with computational fluid dynamics (CFD), which limits the range of applications. On the other hand, the results are computed from measured velocity fields rather than from simulated ones. This allows the investigation of those cases for which the numerical simulation of the flow field would be difficult, because of the uncertainty in the definition of the in-flow and out-flow conditions, or would be expensive, such as high Reynolds number flows and wall-bounded flows over complex geometries. Only recently, few researchers started to investigate the potential of the combination of PIV and acoustic models. Schram,[8] for example, performed phase-locked PIV measurements of a jet of which the periodicity was acoustically triggered (pseudo-time-resolved measurements). Later on, Haigermoser[9] presented time-resolved PIV measurements in combination with Curle's analogy. Despite its innovative character, the work of Haigermoser should be considered as a preliminary study: the experiments were performed in a water flow facility at a low free-stream velocity ($Re = 7.8 \times 10^3$), such conditions are not representative of those for significant acoustic noise generation. Furthermore, his study did not provide any comparison of the estimated sound emission with direct acoustic measurements. In a previous study,[10] we performed combined PIV and acoustic measurements using Curle's analogy to compute the acoustic pressure from the PIV data. The measurements were performed in air and relatively high Reynolds numbers ($Re = 24 \times 10^3 \sim 30 \times 10^3$). The acoustic emission was significant and allowed us to compare the acoustic emission estimated from the PIV data with the sound directly measured by a set of microphones positioned in the acoustic far field. We also performed a detailed analysis and validation of some of the assumptions involved in the derivation of the source term for Curle's analogy, as well as in its application. Moore *et al.*[11] investigated the possibility of using spectral methods for the computation of Curle's analogy source term and compared the solution with the results obtained from the same data analyzed in the time domain. Recent reports,[12–14] including a preliminary and partial description of the results presented here,[15] focus on the application of acoustic analogies to PIV data showing the growing interest in this new technique and pointing out the fact that many aspects still need to be investigated and a number of issues need to be clarified.

In the present study, we compare the application of two different acoustic models to our PIV data: Curle's analogy[16] and the Vortex Sound Theory derived by Powell[17] and developed by Howe,[18] presented here for the first time in combination with the time-resolved PIV data. As a test case for the comparison of the application of these two acoustic analogies to experimental PIV data, we chose to study the flow over a rectangular open[19] cavity. This geometry is well suited for the development and testing of this new experimental technique for the study of aeroacoustics of wall-bounded flows. It generates a strong periodic acoustic emission with large amplitude. Furthermore, the generation of noise by flow over a rectangular cavity is a common benchmark problem for aeroacoustics, and it has been investigated both experimentally and numerically over the last decades.[20] Ahuja and Mendoza[21] showed how the flow over open cavities depend on multiple factors, such as the cavity geometry, the free stream velocity, and the properties of the upstream boundary layer. Gharib and Roshko[22] identified different flow regimes. In particular, they reported that, when the ratio between the cavity length, L, and the boundary layer momentum thickness, θ, falls within certain values ($80 \div 100 \langle L/\theta \rangle 120 \div 140$ depending also on other parameters), the flow passing over the cavity develops in what is known as the "shear layer mode." The shear layer separating at the leading edge of the cavity develops into large-scale coherent spanwise vortices. These vortical structures periodically impinge on the aft wall of the cavity, producing pressure fluctuations that radiate acoustic waves and that generate a self-sustaining oscillation mechanism. This mechanism has a double nature, i.e., acoustic and hydrodynamic. Which one dominates depends on the wavelength of the perturbation and, therefore, on the flow speed and the characteristic dimension of the cavity, i.e. the streamwise length of the cavity. In low-speed flows, the cavity can be considered as acoustically compact; its length is much smaller than the acoustic wavelength. Therefore, the acoustic perturbation is

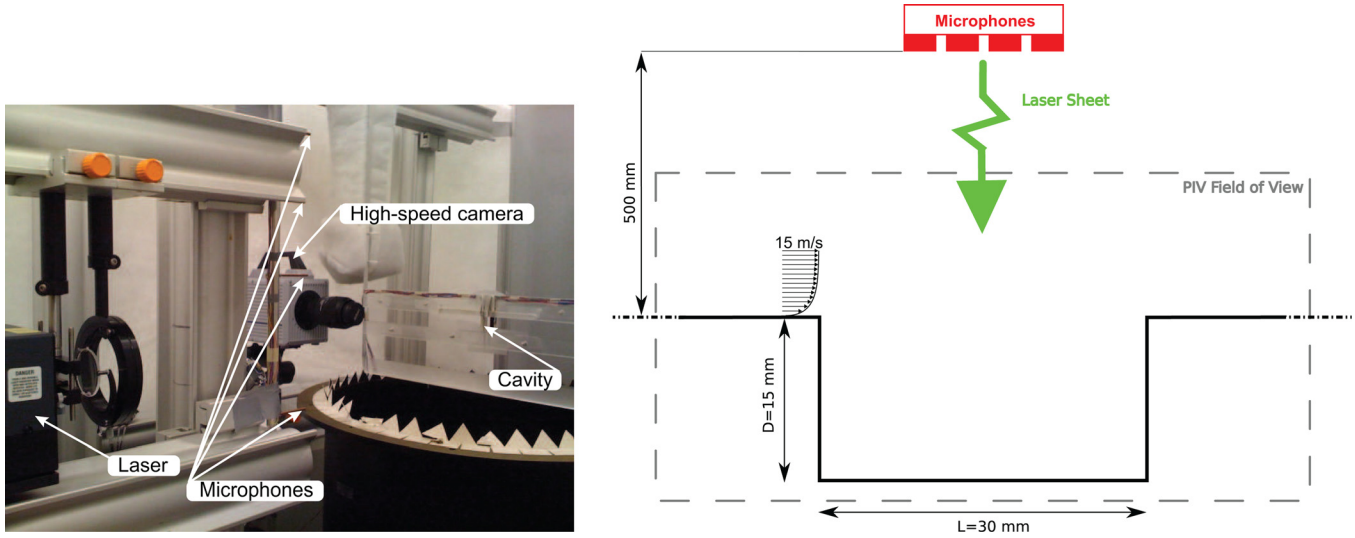

FIG. 1. (Color online) Photo and schematic of the experimental setup.

not able to influence the flow behavior inside the cavity, and hence the self-sustaining oscillation mechanism is purely hydrodynamic. It consists of a recirculating vortex inside the cavity that interacts with the shear layer were it enhances and triggers its destabilization. The assumption of compactness is fundamental in the use of acoustic analogies for the prediction of the sound emission, since it permits to decouple the acoustic features of the flow from the hydrodynamic ones and, therefore, to solve an explicit problem. Rossiter[23] proposed a semi-empirical formula to estimate the frequency of the shear layer instability

$$St = \frac{fL}{U_0} = \frac{m-\gamma}{\frac{1}{k}+Ma}. \quad (1)$$

Here, St is the Strouhal number, f is the frequency of the oscillation, L is the length of the cavity, U_0 is the free-stream velocity, Ma is the Mach number, k is the ratio between the shear layer convection velocity, and the free-stream velocity, $n=1,2,3,\ldots$, is the mode number, and γ an empirical constant that is set to 0.25. Equation (1) has been derived for flows in which the feedback mechanism is of acoustic nature. It does not provide accurate predictions for low Mach numbers ($Ma<0.2$),[24,25] where the flow can be regarded as incompressible and the feedback mechanism is mainly hydrodynamic. Studies at very low Mach number give results that deviate significantly from Rossiter prediction, showing at the same time a broad scattering of the Strouhal number of the oscillation.[25–27] In incompressible flows, the frequency of the oscillation is governed by the convective velocity of the vortices in the shear layer. The convective velocity depends on the properties of the incoming boundary layer, in particular, its momentum thickness. The Strouhal number is commonly defined by the free-stream velocity rather than the convective one, which may explain the scattering of the results. The vorticity in the shear layer, triggered by the mechanism described before, concentrates in an integer number of discrete vortices along the cavity length. The oscillation frequency is therefore simply given by

$$St = \frac{fL}{U_c} = n, \quad (2)$$

where U_c is the shear layer convective velocity. In this case, the hydrodynamic mode n is defined by the number of discrete vortices along the cavity length and is proportional to the inverse of the boundary layer momentum thickness.

II. METHODOLOGY

The study was carried out by means of combined high-speed planar PIV imaging and sound measurements. We performed measurements with a laminar boundary layer flow approaching the cavity, at a free-stream velocity of 15 m/s giving a Reynolds number of 30×10^3, based on the cavity length, L. For the investigated flow condition, the ratio between the length of the cavity and the boundary layer momentum thickness (determined from the velocity profile that was measured by traversing a hot wire anemometer) was $L/\theta=112$. At this condition, the flow passing over the cavity induces the "shear layer mode" described in the introduction. Measurements were conducted in the vertical open-jet wind tunnel of the Low-speed Aerodynamics Laboratories of the Aerospace Department at the Delft University of Technology. The cavity was machined in a flat plate and positioned in the test section aligned with the flow. Figure 1 shows a schematic representation of the experimental configuration including the dimensions of the cavity. The cavity had a width of 600 mm, spanning the full width of the tunnel and giving a width to length ratio of $W/L=20$. Details of the measurements and the experimental conditions are given elsewhere.[10]

A. PIV and microphones

The PIV system consisted of a 12-bit 1024×1024 pixels camera (Photron FastCAM A1S), used at a image format of 512×1024 pixels to allow an increase of the frame rate that matches the minimum required frame rate to resolve the

time-dependent flow, and a dual-cavity pulsed Nd:YLF laser (New Wave Pegasus). The flow was seeded by means of a stage smoke generator (Safex) that produces particles of approximately 1 μm in diameter. PIV image pairs were acquired at a frequency of 3 kHz with a time delay of 65 μs between the first and second frame. This time delay was chosen as an optimum between two opposing demands: it allows enough particle-image displacement between the two frames in the slower regions of our flow inside the cavity (in the order of 2–3 pixels) while keeping it within reasonable limits in the regions with a faster flow (typically 16 pixels in the free-stream area). The laser sheet was estimated to be approximately 1 mm thick, which was determined by projection onto a millimetric scale. This is comparable to the in-plane dimension of our final PIV interrogation window. Data were processed using a multi-pass algorithm.[28] Window deformation[29] was also applied to accommodate the large spatial dynamic range of the flow. The interrogation windows were placed in such a way that their boundaries coincided with the walls of the cavity. The distance between the cavity walls and the location of the first vector is therefore half the size of an interrogation window. The final passes in all domains were done with square interrogation windows of 16×16 pixels with a 50% overlap, giving a vector spacing of 0.48 mm throughout the entire measurement domain.

The emitted sound was recorded with 4 microphones (Sonion serie8000) positioned 0.5 m above the cavity lid plane. The sound pressure was acquired at a frequency of 100 kHz during the acquisition of the PIV data. The analog microphone signals where amplified in order to get an optimum signal dynamic range. The microphones were then calibrated a posteriori by comparison with a calibrated microphone (CESVA P-05) that was exposed together with the other microphones used in the measurement (including the analog signal amplifiers) to the same acoustic field. This field was generated by a signal generator unit and a loudspeaker. We performed measurements for a wide range of amplitudes and frequencies. As specified by the manufacturer of the microphones, the amplitude response appeared to be independent of the frequency within our measurement range (from 100 Hz to 8 kHz). The conversion from electric signal (in volts) to pressure (in pascal) appeared to be given by a linear relation (with a linear regression coefficient, R^2, that is, better than 0.99) and with a zero offset, i.e., the conversion reduces to a single gain coefficient. For further details about the experimental setup, we refer to the paper by Koschatzky *et al.*[10]

B. Acoustic analogies

The emitted sound was computed using both Curle's analogy and Vortex Sound Theory. Both methods were derived from the compressible Navier-Stokes equations rearranged into two different forms of an inhomogeneous wave equation. The compactness assumption made it possible to decouple the acoustic features of the flow from the hydrodynamic ones. Consequently, the acoustic variable and the source term in the wave equation could be regarded as independent, and the problem could be solved explicitly.

In both methods, we took into account the presence of the non-compact wall, in which the cavity was present, by using the image principle in the derivation of the solution. Many studies, both experimental[9,10] and numerical,[30,31] make the simple assumption that it is possible to limit the computation to the source area (in our case, a cavity) and its nearest surroundings. This is because the measured source term appears to decay rapidly away from the source region. In a previous study,[10] we made the same assumption and computed the acoustic pressure fluctuation level in the far field using Eq. (4), in which the surface integral was extended from the cavity to the boundaries of the PIV measurement domain. The pressure fluctuations were windowed,[10] when approaching the boundaries, to avoid erroneous sources due to sharp truncations at the edges of the integration domain. This approach is in general easy to implement and gives reasonably accurate results, but it ignores parts of the solid walls in the far field region where the compactness assumption no longer holds. Even though the source region is compact, the solid body in its proximity is not. Hence, an unknown and potentially significant contribution to the surface integral from the acoustic pressure fluctuation is neglected. Taking into account the presence of a non-compact surface near the compact source of sound is usually not straightforward, since the compactness assumption needs to be given up and the problem becomes explicit. For the particular case of large planar and rigid surfaces, the problem is rather simple, since the image principle can be applied.

The flow under investigation is characterized by the periodic shedding of large structures in the shear layer (the "shear layer mode" described in the introduction). It is well known that these structures are coherent over large distances in the spanwise direction. Recent measurements[10] on this configuration confirmed this. The emitted sound is produced by the unsteady motions of the flow. In particular, at the Mach number under consideration, the only significant contribution comes from the interaction of the turbulent structures with the solid boundaries of the cavity.[16] The largest portion of the emitted sound is due to the large spanwise-coherent structures in the shear layer that produce high intensity tonal sound emissions; the three-dimensional turbulent fluctuations that are superimposed on the two-dimensional periodic flow contribute to the broadband sound spectrum with a much lower intensity, which adds little to the overall sound emission. The results presented here are computed from velocity fields obtained by planar PIV measurements in a streamwise-normal plane. We therefore cannot include any source terms that are based on a contribution of velocity fluctuations in the out-of-plane direction. We compute the flow as a completely two-dimensional flow. At the same time, we approximate the radiation of the sound from the whole cavity by using a single middle plane. It is assumed that the cavity is radiating coherently along the spanwise direction. Both approximations are acceptable, given the large spanwise-coherent structures that are responsible for most of the sound emission. However, the assumptions are not valid for the smaller non-coherent structures that are present in the flow. The effect of these assumptions on the final result is two-

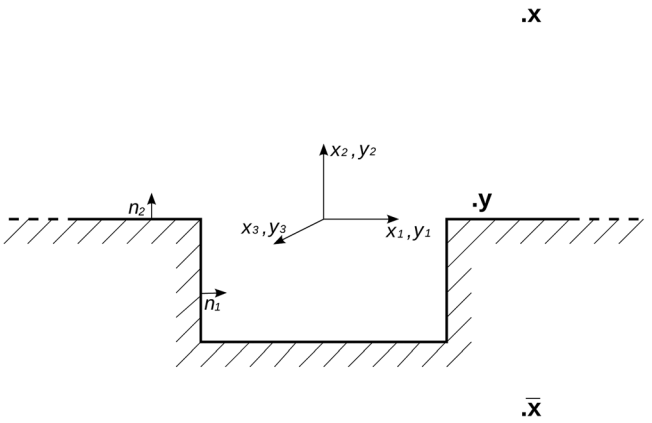

FIG. 2. Coordinate system and notation used in this paper. $\mathbf{y}$ is the source location, $\mathbf{x}$ is the listener location, and $\bar{\mathbf{x}} = (x_1, -x_2, x_3)$ is its image on the opposite side of the wall.

fold: the broadband sound spectrum is underestimated by considering only a part of the total turbulence in the calculation of the sound source terms, while on the other hand, it tends to be overestimated by considering every fluctuation as coherent in the spanwise direction as they become smaller. We expect the effects to become more significant at higher frequencies, since we conjecture that the turbulent structures are less coherent in the spanwise direction, the smaller they are. In the end, the broadband contribution to the overall sound emission is very small compared to the tonal component, and therefore we anticipate that the final result is not significantly affected by our assumptions.

Figure 2 summarizes the coordinate system and notation used in the analogies: $\mathbf{y}$ is the source location, $\mathbf{x}$ is the listener location, and $\bar{\mathbf{x}} = (x_1, -x_2, x_3)$ is its image on the opposite side of the wall. Subscripts i = 1, 2, and 3 refer to the streamwise, normal, and spanwise directions, respectively. The assumption of a listener positioned in the far field implies that $|\mathbf{x}| \to \infty$ and $|\mathbf{x}| \gg |\mathbf{y}|$. The assumption of compactness implies that $l \ll \lambda$, where l is the typical source dimension and λ the characteristic wavelength of the emitted sound. Under both assumptions, it follows that $|\mathbf{y}| \sim l$ and $\lambda \geq |\mathbf{x}|$.

1. Curle's analogy

We first considered Curle's analogy[16] for the computation of the acoustic pressure from the PIV data. Curle's acoustic analogy derives from Lighthill's analogy,[32] where the chosen acoustic variable is the perturbation density $\rho - \rho_0$. In case of stationary and rigid bodies, Curle's analogy takes the form

$$a_0^2(\rho - \rho_0) = \frac{\partial^2}{\partial x_i \partial x_j} \int_V [T_{ij}] \frac{d^3\mathbf{y}}{4\pi|\mathbf{x}-\mathbf{y}|} - \frac{\partial}{\partial x_i} \oint_S [(p-p_0)\delta_{ij} - \sigma_{ij}] \frac{dS_j(\mathbf{y})}{4\pi|\mathbf{x}-\mathbf{y}|}, \quad (3)$$

where a_0 is the speed of sound, $(\rho - \rho_0)$ is the fluctuating fluid density, V is the source region volume, T_{ij} is the Lighthill stress tensor, $|\mathbf{x}-\mathbf{y}|$ is the distance between the source and the listener positions, S_j is the surface of the rigid body with the normal pointing into the flow region in the *j-th* direction, $(p - p_0)$ is the fluctuating pressure at the surface, and σ_{ij} is the viscous stress tensor. The terms in the square brackets in Eq. (3) need to be evaluated at the retarded time, $t - |\mathbf{x}-\mathbf{y}|/a_0$. At low Mach number, the perturbation pressure can be expressed as $p - p_0 = (\rho - \rho_0)a_0^2$. Under the same assumption, in high Reynolds numbers flows and for listeners positioned in the far field, Curle's equation can be further simplified: the volume integral can be ignored, as well as the viscous terms, and a far-field approximation can be adopted. It is also convenient to replace the spatial derivative $\partial/\partial x_j$ with the temporal derivative $\partial/\partial t$. One thus obtains

$$p(\mathbf{x},t) - p_0 = \frac{x_i}{4\pi a_0|\mathbf{x}|^2}\frac{\partial}{\partial t} \oint_S (p-p_0)\left(\mathbf{y}, t - \frac{|\mathbf{x}|}{a_0} + \frac{\mathbf{x}\cdot\mathbf{y}}{a_0|\mathbf{x}|} + O\left(\frac{|\mathbf{y}|}{|\mathbf{x}|}\right)^2\right) dS_i(\mathbf{y}). \quad (4)$$

Under the assumption of a listener positioned in the far field region, the terms of order $O\left(\frac{|\mathbf{y}|}{|\mathbf{x}|}\right)^2$ and higher can be safely ignored. To take into account the presence of the non-compact wall that contains the cavity we followed the approach introduced by Powell;[33] we applied Curle's solution both at the observer point $\mathbf{x}$ and at its image $\bar{\mathbf{x}}$ on the opposite side of the wall,

$$p(\mathbf{x},t) - p_0 = \frac{x_i}{4\pi a_0|\mathbf{x}|^2}\frac{\partial}{\partial t} \oint_S (p-p_0)\left(\mathbf{y}, t - \frac{|\mathbf{x}|}{a_0} + \frac{\mathbf{x}\cdot\mathbf{y}}{a_0|\mathbf{x}|}\right) dS_i(\mathbf{y}) \quad (5)$$

in the far field and

$$0 = \frac{\bar{x}_i}{4\pi a_0|\mathbf{x}|^2}\frac{\partial}{\partial t} \oint_S (p-p_0)\left(\mathbf{y}, t - \frac{|\bar{\mathbf{x}}|}{a_0} + \frac{\bar{\mathbf{x}}\cdot\mathbf{y}}{a_0|\mathbf{x}|}\right) dS_i(\mathbf{y}) \quad (6)$$

at the image location. The two solutions were then added together. If the cavity can be considered as acoustically compact, it is possible to safely discard the retarded time variations $\frac{\mathbf{x}\cdot\mathbf{y}}{a_0|\mathbf{x}|}$ and $\frac{\bar{\mathbf{x}}\cdot\mathbf{y}}{a_0|\mathbf{x}|}$ for the sound sources within the cavity region. These must be retained along the non-compact walls before and after the cavity. With $\mathbf{x} = (x_1, x_2, x_3)$, $\bar{\mathbf{x}} = (x_1, -x_2, x_3)$, and $|\bar{\mathbf{x}}| = |\mathbf{x}|$, it follows that the contribution to the sound emission from pressure fluctuations at walls with the normal pointing in the $i = 2$ direction cancels out. In contrast, the terms for the walls with the normal pointing in the $i = 1$ and $i = 3$ directions contribute with a double intensity of that in the free-space solution. This means that the walls upfront and after the cavity and the bottom of the cavity are "silent," and the sound is produced only by pressure fluctuations at the vertical walls of the cavity. Curle's equation then takes the form

$$p(\mathbf{x},t) - p_0 = \frac{x_i}{2\pi a_0|\mathbf{x}|^2} \int_S \frac{\partial p}{\partial t}\left(\mathbf{y}, t - \frac{|\mathbf{x}|}{a_0}\right) dS_i(\mathbf{y}), \quad (7)$$

where $i = 1,3$. In the derivation of Eq. (7), we moved the time derivative inside the integration. This choice was

imposed by the method with which the time derivatives were computed and that will be explained in the next paragraph. The index i is in the principle either 1 or 3, but in the present experimental configuration, there are no walls with a normal component in the $i=3$ direction. Therefore, the index to consider here is in practice just $i=1$. Equation (7) relates the acoustic pressure at the listener position, $\mathbf{x}$, to a surface integral of the time derivative of the hydrodynamic wall pressure. The integral is limited to the vertical walls of the cavity and needs to be evaluated at a retarded time that takes into account the distance between the source and the listener position.

To compute the pressure and its time derivative at the walls, we solved a Poisson equation for the pressure derived from the momentum equation. The viscous terms were ignored because of the relatively high Reynolds of the flow under consideration (see Liu and Katz[34] and Koschatzky *et al.*[10]). The Poisson equation for the pressure is

$$\nabla^2 p = -\rho_0 \nabla \cdot \left(\frac{D\mathbf{u}}{Dt}\right), \tag{8}$$

where p is the pressure, ρ_0 is the fluid density, and $\mathbf{u}$ is the velocity vector field. As explained earlier in this section, together with the implications of such an approximation, only the streamwise and normal velocity components are available. Therefore, the flow is treated as two-dimensional. Neumann and Dirichlet boundary conditions were applied at the boundaries of the domain

$$\begin{cases} \dfrac{\partial p}{\partial y_1} = -\rho_0 \dfrac{Du_1}{Dt}, & \text{on } y_1 = \text{constant boundaries}, \\ \dfrac{\partial p}{\partial y_2} = -\rho_0 \dfrac{Du_2}{Dt}, & \text{on } y_2 = \text{constant boundaries}, \\ p = \dfrac{1}{2}\rho_0 \left(U_0^2 - \mathbf{u}^2\right), & \text{at the upper boundary of the domain}, \end{cases} \tag{9}$$

where y_1 and y_2 are the in-plane coordinate directions (see Figure 2 for the definition of the coordinate reference system), and u_1 and u_2 are the corresponding velocity components. A validation of the pressure reconstruction by means of a comparison with wall-pressure measurements is provided by Koschatzky *et al.*[10]

The velocity material derivatives are computed directly, using the method proposed by Liu and Katz[34] and further developed by Moore *et al.*[11] The method consists of the evaluation of the total derivative of the velocity by tracking a fluid parcel by means of a Lagrangian approach, under the assumption of Taylor's hypothesis of frozen turbulence. This is permitted, since the characteristic fluctuations of the flow are small with respect to the characteristic velocity of the mean recirculating flow in the cavity, and therefore the larger structures, which are primarily responsible for the total sound emission, convect without much deformation within the duration of our acquisition. This approach was necessary due to the relatively large time steps between PIV snapshots, which did not allow for a correct computation of time derivatives when done in the conventional Eulerian way. Figure 3(a) shows a region of the flow close to the trailing upper corner of the cavity. The instantaneous vector field is displayed together with the backward and forward paths for one vector and the corresponding positions and velocity vectors at the previous and subsequent time steps. These were computed by subdividing the time interval between subsequent time steps in smaller sub-steps, by interpolating the velocities field at the sub-steps, and by computing the displacement for every vector location during the sub-steps. Figure 3(b) shows the statistical correlation between the velocity magnitude field, U, at a certain time steps and the velocity magnitude field obtain by computing the path from the previous time step, U_{ps}, over the whole data set. Data are normalized by the free-stream velocity, U_0. It can be seen that the localization of the displacement is extremely accurate allowing for a correct computation of the velocity material derivative using a central differences scheme. The pressure material derivative is computed in the same way as the velocity material derivatives, and the pressure time derivative is simply obtained by

$$\frac{\partial p}{\partial t} = \frac{Dp}{Dt} - \mathbf{u} \cdot \nabla p. \tag{10}$$

For further details on the computation of the pressure and of the pressure time derivative, we refer to a paper by Koschatzky *et al.*[10]

2. Vortex Sound Theory

Powell[17] derived a different form of Lighthill's analogy by considering the total enthalpy, B, instead of the fluid density, ρ, as the acoustic variable. Howe[18] generalized Powell theory, extending its application to wall bounded flows. At low Mach number and in the far field, the acoustic pressure $p-p_0$ can be expressed in terms of the total enthalpy B as $p-p_0=\rho_0 B$. It is therefore possible to solve the acoustic equation for the perturbation pressure by means of a Green's function in a similar way as done in the derivation of Curle's analogy. The main difference is that, while in the derivation of Curle's analogy, the solution was found in free space and the solid body with its boundaries was introduced successively (leading to a surface integral term), here the presence of the solid boundary is a part of the wave equation solution itself, since we used a Green's function tailored to the cavity geometry. Under the same assumptions made in the derivation of Curle's analogy, i.e. of a stationary and rigid body and of a low Mach and high Reynolds numbers flow, it can be found that[18]

$$p(\mathbf{x},t) - p_0 = -\rho_0 \int_{-\infty}^{+\infty} \int_V (\boldsymbol{\omega} \times \mathbf{u})(\mathbf{y},\tau) \nabla G(\mathbf{x},\mathbf{y},t-\tau) dV d\tau. \tag{11}$$

In Eq. (11), ρ is the fluid density, $\boldsymbol{\omega} \times \mathbf{u}$ is the Lamb vector, i.e. the cross product of vorticity $\boldsymbol{\omega}$ and velocity $\mathbf{u}$, and ∇G is the gradient of the Green's function with respect to $\mathbf{y}$. In the derivation of the tailored Green's function, as for Curle's analogy, we took into account the presence of the non-compact wall in which the cavity was located. We did this by considering the Green's function solution for a flat plate, derived by means of the image principle (Eq. (12)) and by

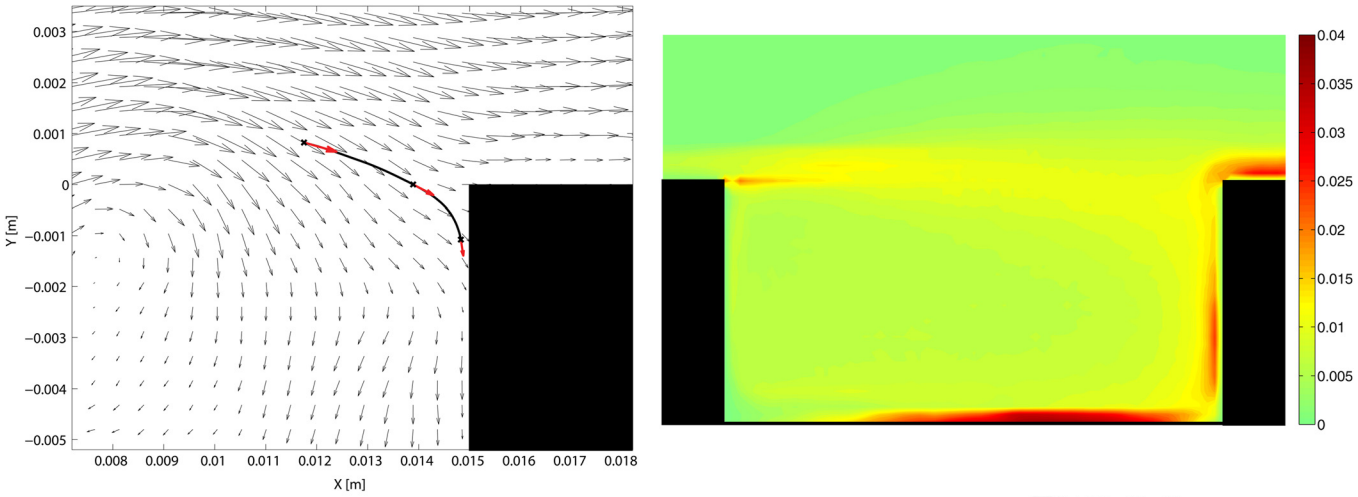

(a)A pathline (b)Statistical correlation: $\frac{\sum_1^n |(U-U_{ps})|}{nU_0}$

FIG. 3. (Color online) Instantaneous vector field with one pathline and statistical validation.

expanding this solution to first order in $\mathbf{y}$ near the cavity (Eq. (13)), i.e. correcting to dipole order:[18]

$$G(\mathbf{x},\mathbf{y},t-\tau) = \frac{1}{4\pi|\mathbf{x}-\mathbf{y}|}\delta\left(t-\tau-\frac{|\mathbf{x}-\mathbf{y}|}{a_0}\right) + \frac{1}{4\pi|\bar{\mathbf{x}}-\mathbf{y}|}\delta\left(t-\tau-\frac{|\bar{\mathbf{x}}-\mathbf{y}|}{a_0}\right) \tag{12}$$

$$= \frac{1}{4\pi|\mathbf{x}|}\left[2\delta\left(t-\tau-\frac{|\mathbf{x}|}{a_0}\right) + \frac{(\mathbf{x}+\bar{\mathbf{x}})\cdot\mathbf{y}}{a_0|\mathbf{x}|}\delta'\left(t-\tau-\frac{|\mathbf{x}|}{a_0}\right)\right] + O\left(\frac{|\mathbf{y}|}{|\mathbf{x}|}\right)^2. \tag{13}$$

As for Curle's analogy, under the far field assumption, the terms of order $O\left(\frac{|\mathbf{y}|}{|\mathbf{x}|}\right)^2$ and higher can be safely ignored. We then tailor the Green's function on the cavity geometry in such a way that its normal derivatives as a function of y vanish at the walls. For a compact source such as our cavity, this is easily done by correcting in Eq. (13) the term

$$(\mathbf{x}+\bar{\mathbf{x}})\cdot\mathbf{y} \quad \text{with} \quad (\mathbf{x}+\bar{\mathbf{x}})\cdot\mathbf{Y} \equiv 2\mathbf{x}\cdot\mathbf{Y}. \tag{14}$$

The term $\mathbf{Y}$ is the Kirchhoff vector for the body. To this order of approximation, the components Y_i of the Kirchhoff vector satisfy the Laplace equation $\nabla^2\mathrm{Y}_i = 0$, with $\partial\mathrm{Y}_i/\partial y_n = 0$ at the surface of the body, fulfilling the boundary conditions of the Green's function in the presence of a solid body. For a detailed interpretation of $\mathbf{Y}$, we refer to the work of Howe.[18,35] The Green's function (13) then becomes

$$G(\mathbf{x},\mathbf{y},t-\tau) = \frac{1}{2\pi|\mathbf{x}|}\left[\delta\left(t-\tau-\frac{|\mathbf{x}|}{a_0}\right) + \frac{x_i\mathrm{Y}_i}{a_0|\mathbf{x}|}\delta'\left(t-\tau-\frac{|\mathbf{x}|}{a_0}\right)\right], \tag{15}$$

and therefore the gradient ∇G of the Green's function with respect to $\mathbf{y}$ is

$$\nabla G(\mathbf{x},\mathbf{y},t-\tau) = \frac{x_i}{2\pi|\mathbf{x}|^2}\nabla\mathrm{Y}_i\delta'\left(t-\tau-\frac{|\mathbf{x}|}{a_0}\right), \tag{16}$$

since $\mathbf{Y}$ is the only term that is a function of $\mathbf{y}$. Equation (11) then finally takes the form

$$p(\mathbf{x},t)-p_0 = -\frac{\rho_0 x_i}{2\pi a_0|\mathbf{x}|^2}\int_V\left[\frac{\partial}{\partial t}\left((\boldsymbol{\omega}\times\mathbf{u})\cdot\nabla\mathrm{Y}_i(\mathbf{y})\right)\right]dV(\mathbf{y}), \tag{17}$$

with $i=1,3$. As for Curle's analogy, i is either 1 or 3. The components Y_i can be interpreted as the velocity potentials of an incompressible flow past the cavity, having unit speed in the i-th direction at large distances from the cavity. Since $|\nabla\mathrm{Y}_3(\mathbf{y})| \ll |\nabla\mathrm{Y}_1(\mathbf{y})|$, we consider only $i=1$. Y_1 is found by conformal mapping of the region above the cavity cross-section on a half plane,[36] where the solution for the velocity potential is straightforward. In particular, the Schwarz-Christoffel transformation states that

$$\mathrm{Y}_1(\mathbf{y}) = \Re\left(\frac{Lk}{2E(k)}\xi(\mathbf{y})\right) \quad \text{and} \quad \mathbf{y} = \frac{L}{2E(k)}E(\xi,k). \tag{18}$$

In Eq. (18), $\mathbf{y} = y_1 + iy_2$ and $\xi = \xi_1 + i\xi_2$ (as in Figure 4), and $\Re(\cdot)$ indicates the real part of the argument, L is the cavity length, k is a parameter for the aspect ratio of the cavity,[36] $E(k)$ is a complete elliptical integral of the second kind, and $E(\xi,k)$ is an incomplete elliptical integral of the second kind.[37] Figure 4 shows streamlines and equipotential lines obtained by conformal mapping of the region above the cavity (plane y) into a half plane (plane ξ). The terms within the square brackets in Eq. (17) need to be evaluated at the retarded time, $t-|\mathbf{x}|/a_0$. Equation (17) relates the acoustic pressure at the listener position, $\mathbf{x}$, to a volume integral of the time derivative of the Lamb vector, evaluated at a retarded time that takes into account the distance between the

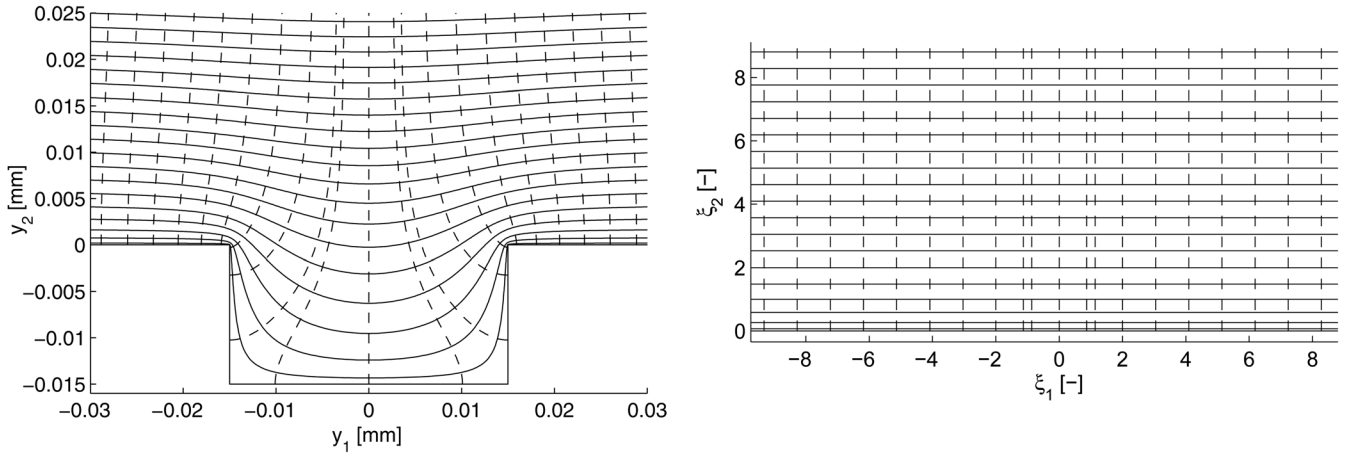

(a)Plane y (b)Plane ξ

FIG. 4. Streamlines (—) and equipotential lines (- -) in the y and ξ planes.

source position and the listener position. The problem then reduced to the computation of the Lamb vector and its time derivative. The experimental data used for the estimation of the emitted sound were planar, i.e. only the components u_1 and u_2 of the velocity field and the component ω_3 of the vorticity field were available. Therefore, some of the terms in the volume integral of Eq. (17) are missing. In particular, since

$$(\boldsymbol{\omega}\times\mathbf{u})\cdot\nabla \mathrm{Y}_1 = (\omega_2 u_3 - \omega_3 u_2)\frac{\partial \mathrm{Y}_1}{\partial y_1} + (\omega_3 u_1 - \omega_1 u_3)\frac{\partial \mathrm{Y}_1}{\partial y_2} + (\omega_1 u_2 - \omega_2 u_1)\frac{\partial \mathrm{Y}_1}{\partial y_3}, \tag{19}$$

and $\partial \mathrm{Y}_1/\partial y_3 = 0$ (by definition), the terms that could not be evaluated from the planar PIV data were $\omega_2 u_3$ and $\omega_1 u_3$. The flow under examination is quasi two-dimensional,[10] which implies $|\omega_3| \gg |\omega_2|, |\omega_1|$ and $|u_3| \ll |u_1|, |u_2|$. The results that were obtained, while ignoring the terms we did not dispose of, could therefore be seen as a good approximation of the complete results as discussed earlier in this section. The time derivative was computed in a Lagrangian reference frame to deal with the relatively large time steps between PIV snapshots (as for the time derivative in Curle's analogy).

III. RESULTS

A. PIV results

The mean flow in the cavity is characterized by a large clockwise rotating flow region in one part of the cavity and a smaller recirculation region in the lower left corner of the cavity (see Figure 5). The recirculating flow inside the cavity impinges on the separating laminar shear layer, which determines its de-stabilization and triggers the development of vortical structures that convect downstream and then impinge on the aft vertical cavity wall. The shedding of the shear layer is shown in Figure 7, where three consecutive

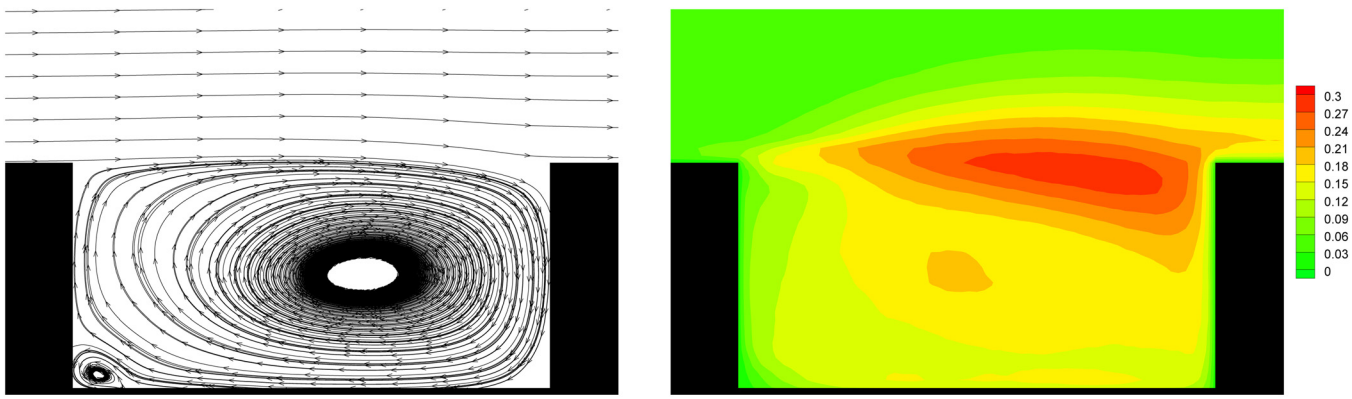

(a)Streamlines (b)Turbulent intensity normalized to the free stream velocity

FIG. 5. (Color online) (a) Mean flow in the cavity, represented as streamlines. (b) Turbulent intensity.

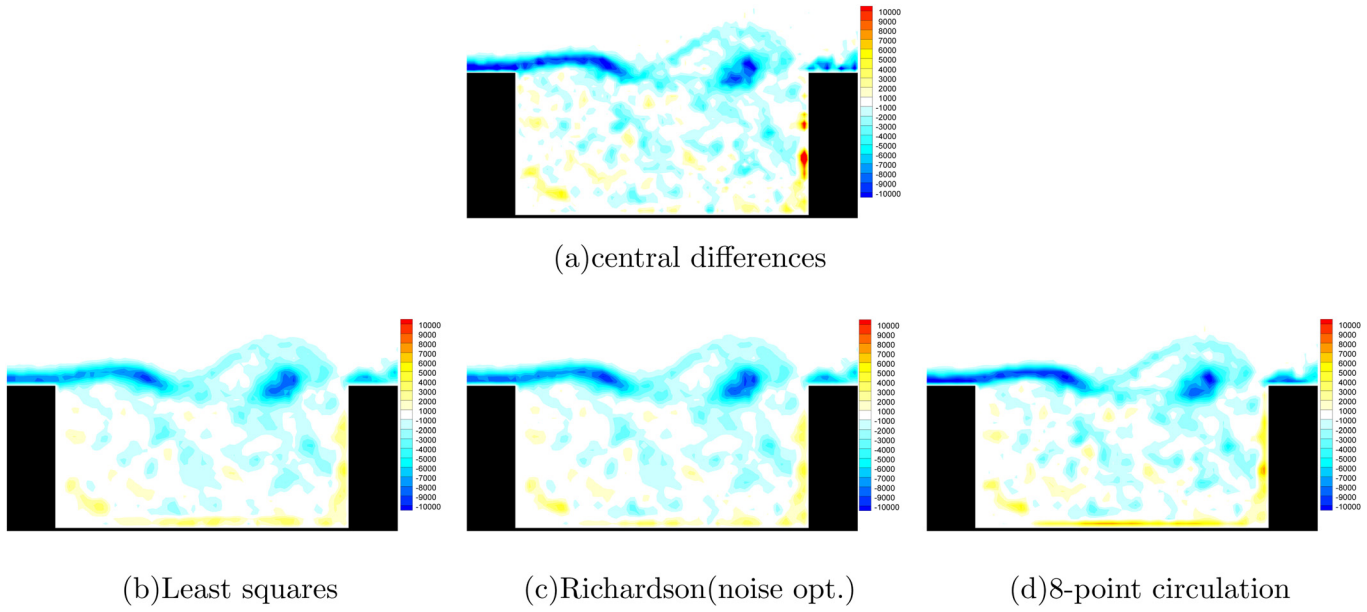

FIG. 6. (Color online) Out-of-plane vorticity [1/s] computed by different differentiation schemes.

snapshots are depicted (this also gives an indication of the temporal resolution that was achieved in this measurement). The contours in Figure 7(a) indicate the out-of-plane component of the vorticity, ω_3.

As vorticity is part of the source term in the Vortex Sound Theory (Eq. (19)), reliable quantitative measurements are necessary. Obtaining reliable differential quantities, such as vorticity, from the PIV data is not straightforward. In general, PIV data can be quite noisy when compared, for example, to CFD data, and the spatial resolution may also be limited. Moreover, in our experiment, adjacent data were obtained from overlapping interrogation windows (with an overlap of 50%), so errors in adjacent data are statistically correlated. A standard central difference scheme would therefore increase the uncertainty of the vorticity measurement data with respect to the one computed from an equally noisy but uncorrelated velocity field.[38] In order to reduce the uncertainty in the measurement of the vorticity field, we therefore need to use a more refined approach. Foucaut and Stanislas[39] reviewed several differentiation schemes applied to PIV data for the computation of the out-of-plane vorticity component. They estimate the error, due to truncation, and the effect of measurement noise, as a function of the ratio between the radius of an Oseen vortex and the data spatial resolution. According to their study, the schemes that would have the best performance for the present data are the 4-th order Richardson scheme (optimized for noise reduction), the least square scheme, and the eight-point circulation scheme. Figure 6 shows the out-of-plane vorticity field for one snapshot computed with these methods, and by a standard second order central difference scheme for comparison, while Table I summarizes the mathematical formulations. It turned out that the preferred method is the eight-point circulation scheme. According to Foucaut and Stanislas,[39] this scheme performs well over a broader range of vortex sizes offering a good compromise between

TABLE I. Numerical difference schemes for the computation of the out-of-plane vorticity component from the planar PIV data. ε_u is the error on the velocity and Δx is the spatial resolution.

Scheme	Implementation	Accuracy	Uncertainty
Central differences	$\omega_{3(i,j)} = \frac{u_{2(i+1,j)} - u_{2(i-1,j)}}{2\Delta x_1} - \frac{u_{1(i,j+1)} - u_{1(i,j-1)}}{2\Delta x_2}$	$O(\Delta x^2)$	$\approx 0.71 \frac{\varepsilon_u}{\Delta x}$
Least squares	$\omega_{3(i,j)} = \frac{2u_{2(i+2,j)} + u_{2(i+1,j)} - u_{2(i-1,j)} - u_{2(i-2,j)}}{10\Delta x_1} - \frac{2u_{1(i,j+2)} + u_{1(i,j+1)} - u_{1(i,j-1)} - u_{1(i,j-2)}}{10\Delta x_2}$	$O(\Delta x^2)$	$\approx 0.32 \frac{\varepsilon_u}{\Delta x}$
Richardson (noise opt.)	$\omega_{3(i,j)} = \frac{1}{1239}\left[\left(\frac{272(u_{2(i+1,j)} - u_{2(i-1,j)})}{2\Delta x_1} + \frac{1036(u_{2(i+2,j)} - u_{2(i-2,j)})}{4\Delta x_1} - \frac{69(u_{2(i+8,j)} - u_{2(i-8,j)})}{16\Delta x_1}\right) - \left(\frac{272(u_{1(i,j+1)} - u_{1(i,j-1)})}{2\Delta x_2} + \frac{1036(u_{1(i,j+2)} - u_{1(i,j-2)})}{4\Delta x_2} - \frac{69(u_{1(i,j+8)} - u_{1(i,j-8)})}{16\Delta x_2}\right)\right]$	$O(\Delta x^4)$	$\approx 0.33 \frac{\varepsilon_u}{\Delta x}$
8-point circulation	$\omega_{3(i,j)} = \frac{1}{8\Delta x_1 \Delta x_2}[\Delta x_1(u_{1(i-1,j-1)} + 2u_{1(i,j-1)} + u_{1(i+1,j-1)}) + \Delta x_2(u_{2(i+1,j-1)} + 2u_{2(i+1,j)} + u_{2(i+1,j+1)}) - \Delta x_1(u_{1(i+1,j+1)} + 2u_{1(i,j+1)} + u_{1(i-1,j+1)}) - \Delta x_2(u_{2(i-1,j+1)} + 2u_{2(i-1,j)} + u_{2(i-1,j-1)})]$	$O(\Delta x^2)$	$\approx 0.61 \frac{\varepsilon_u}{\Delta x}$

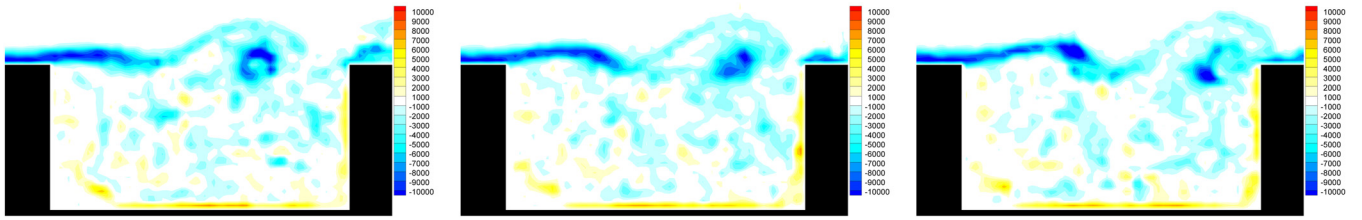

(a)Out of plane vorticity [1/s]

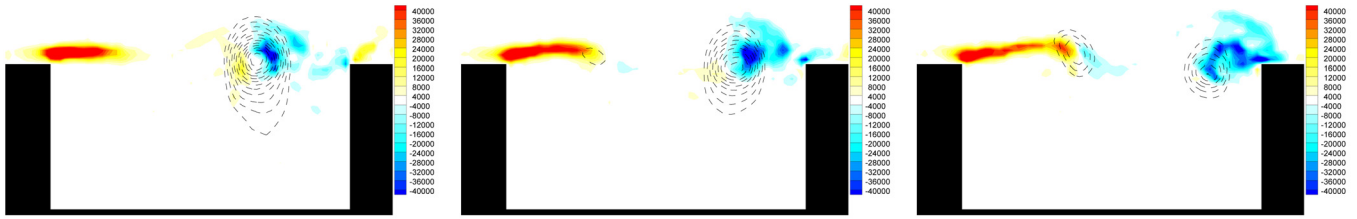

(b)$(\boldsymbol{\omega} \times \mathbf{u}) \cdot \nabla \mathbf{Y_1}$ [m/s^2] (Flood) and pressure [Pa] (Lines)

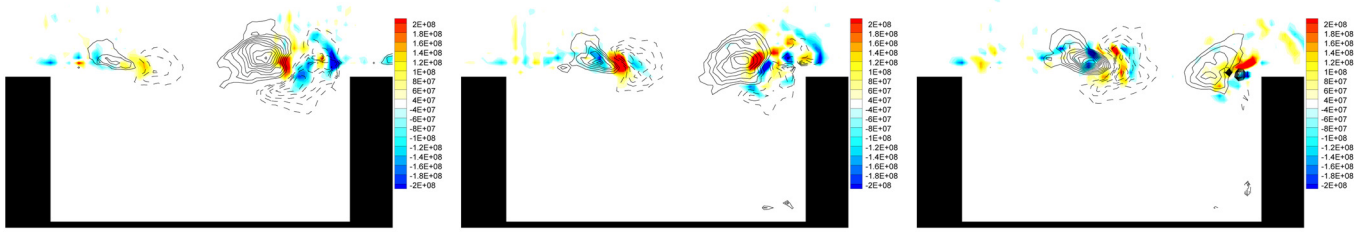

(c)∂/∂t $[(\boldsymbol{\omega} \times \mathbf{u}) \cdot \nabla \mathbf{Y_1}]$ [m/s^3] (Flood) and ∂p/∂t [Pa/s] (Lines)

FIG. 7. (Color online) Three consecutive time steps with $\Delta t = 0.32$ ms.

excessive smoothing and errors due to noise and truncation. It is also the most compact method between the considered ones, allowing a straightforward estimate of vorticity near the walls. Moreover, it is the only method that solves the problem of the correlated adjacent data since no differences of neighboring points are used in the computation, and therefore the bias due to the overlapping of the interrogation data becomes negligible. The method consists of calculating the out-of-plane vorticity value at every data point by computing the circulation from the 8 neighboring points and dividing the result by the enclosed area. This procedure is actually equivalent to computing

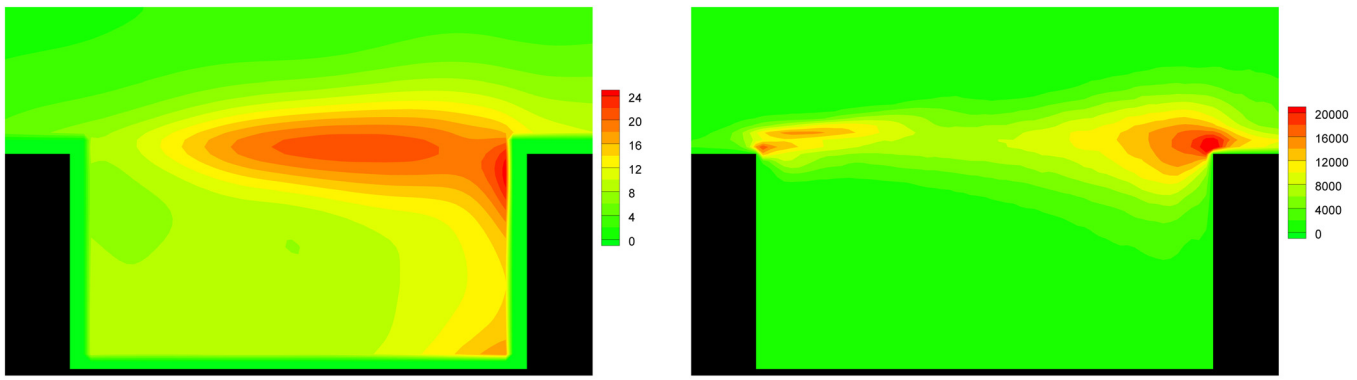

(a)rms of pressure [Pa] (b)rms of $(\boldsymbol{\omega} \times \mathbf{u}) \cdot \nabla \mathbf{Y_1}$ [m/s^2]

FIG. 8. (Color online) Root mean square of the source terms for Curle's analogy (a) and Vortex Sound Theory (b).

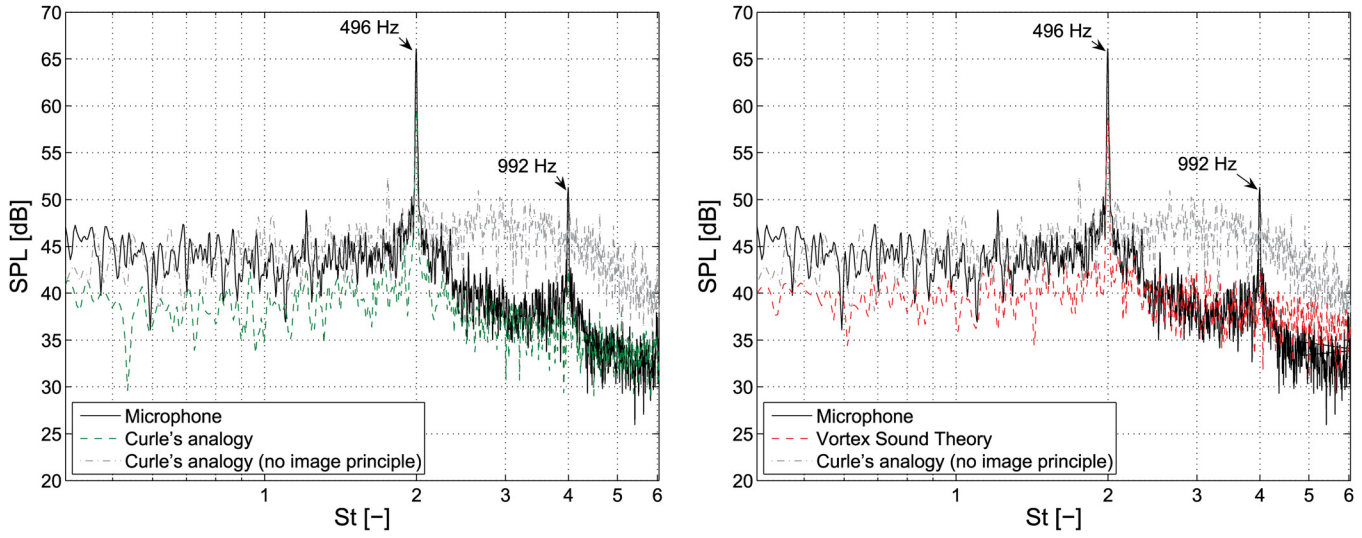

(a)Curle's analogy (b)Vortex Sound Theory

FIG. 9. (Color online) Power spectra of the sound signal from a microphone and of the sound signal computed from the PIV data at the same locations with the two analogies. $St = fL/U_c$ as defined in Eq. (2).

the vorticity field by applying a central difference scheme to a velocity field, that is, first smoothed with a 3×1 points kernel.[40]

Curle's analogy is less critical with respect to the computation of the source term. The Poisson equation from which the pressure field is obtained needs to be solved by integrating over the entire domain. Any localized error is therefore spread to the entire domain and, consequently, the computation of the pressure time derivative is less affected by noise in the individual data.

Figure 7(b) represents the Lamb vector by the Kirchhoff vector (flood) with pressure (lines), and Figure 7(c) represents their respective time derivatives, i.e., the source terms for the two analogies. It is clear how the source areas nicely fall on top of each other. Figure 8 shows the root mean square of the pressure and of the vector product of the Lamb vector and the Kirchhoff vector. These contours represent the magnitude of the variation in the terms in the source region. They therefore give an indication of the areas where most of the emitted sound is produced according to the two analogies (note that for Curle's analogy, the sound source is the pressure fluctuation at the walls and not in the volume). These data, however, do not take into account the time scales during which such variations occur, and thus should be interpreted with an eye on the flow dynamics. For example, the contour levels of the root mean square pressure in Figure 8(a) show relative high values at the lower right corner of the cavity. These variations are actually due to the extremely slow fluctuation of the large recirculation region inside the cavity and not to the much faster turbulent variations (Figure 5). That is why they do not appear in Figure 8(b). Therefore, the pressure time derivatives are very small and do not give a significant sound source contribution. The contours show that both methods detect the trailing upper edge corner of the cavity as the main source of the sound, which is consistent with what has been found in previous studies.[20–22,25,31,41,42] It should be noted that the data are not available down to the wall for the pressure (Figure 8(a)). The pressure field was found integrating a Poisson equation for which the pressure spatial derivatives are given by the equations for the conservation of momentum. The pressure is therefore a function of the material derivatives of the velocity that needs to be calculated with the Lagrangian approach described in Sec. II. It follows that the distance from the wall up to the location where the data are available depends on the typical displacement of particles during a time step. This is a critical aspect in the application of Curle's analogy; the source term is the pressure fluctuation at the wall that is approximated by the values at the closest position available to the wall. This is a reasonable approximation only if the mean streamlines are nearly parallel to the wall and if the position taken into consideration is close enough to the wall to be considered within the wall boundary layer. One must be careful then, when applying Curle's analogy, that the time steps are smaller than the ratio between the boundary layer thickness of the wall and the local velocity.

B. Results obtained with the acoustic analogies

Figure 9 shows the power spectra of a microphone positioned 0.5 m above the cavity (for the position refer to Figure 11) and of the acoustic signal computed with Curle's analogy (in green, dashed) and Vortex Sound Theory (in red, dashed) at the same location. It also shows the power spectrum

TABLE II. Overall sound pressure levels in dB at the microphone position.

Microphone	Curle's analogy	Vortex Sound Theory
76.2	70.0	70.4

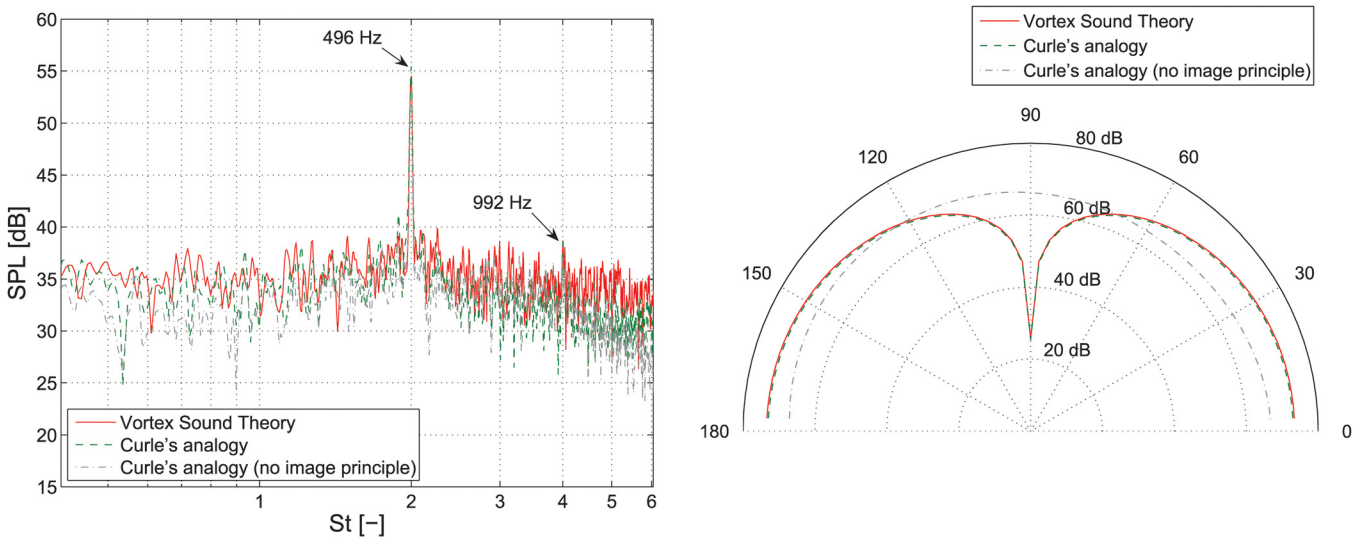

(a)R=1.5m, $\theta = \pi/4$ (b)R=1.5m

FIG. 10. (Color online) Power spectra from the PIV data in the far field and directivity plot at the same distance. $St = fL/U_c$ as defined in Eq. (2).

computed with Eq. (4) (in gray, dot-dashed), which is Curle's analogy without the use of the image principle to account for the non-compact wall in which the cavity take place. The power spectra shown in the graphs are the averages of the power spectra of segments of the original time signals. Each time signal was divided in 8 segments of equal length with a 50% overlap. Each segment was then windowed with a Hamming window of the same length as the segment. The power spectrum of each individual segment was computed through the fast Fourier transform algorithm, and finally, the power spectra of all segments were averaged to reduce the variance in the estimated power spectrum.[43] It should be noted that the experimental facility in which we performed the measurements is not acoustically insulated, even though it can be considered rather quiet with respect to other similar facilities. In addition, due to physical restrictions of the experimental setup, it was not possible to position the microphone at a much larger distance in the far field. The location chosen is almost one typical wavelength[44] away from the cavity. Therefore, the microphone recordings should be taken rather as an indication of the far-field sound level and not as a direct validation for our method. Comparing the estimate of the emitted sound obtained by applying the acoustic analogies to the PIV data and the microphone records, it is possible to see that both the main frequency peak and the first harmonic peak are detected by the two approaches. The main frequency peak corresponds to the second hydrodynamic mode of Eq. (2) and falls in the range reported in other theoretical,[24] experimental,[9,21,45] and numerical[25] studies. The Vortex Sound Theory seems to suffer from a higher broadband noise disturbance in the signal at the very high frequencies. This is probably due to the difficulties described previously in reducing the noise error while computing the source term for the Vortex Sound Theory result. Table II displays the measured overall sound pressure levels at the microphone location. Estimates from Curle's analogy and Vortex Sound Theory are close to each other, but are significantly lower than the measured sound pressure level. The main differences occur at the frequencies below that of the main tonal component. In the low-frequency range, the microphone measurement includes low-frequency disturbances from the testing equipment (like cooling fans and the pump driving the water cooling system of the laser). In the range of frequencies close to the tonal component, we believe that, due to the dimensions of the wind tunnel used in the measurements, standing waves are likely to be present, which amplifies the microphone signal in that specific range of frequencies. The microphones are probably recording higher sound intensities than they should be, explaining the discrepancy with the analogies predictions at the tonal frequency. Figure 10 shows the power spectra computed with the two analogies far enough from the cavity to be considered in the far field and the directivity plot at the same distance. As in Figure 9, we include the results computed with Curle's analogy, but without using the image principle to properly take care of the non-compact wall in which the cavity occurs. This signal, at the displayed location, shows a tonal emission with a much lower intensity than the other results (Figure 10(a)). For those, the same small differences in the spectral distribution remain as in the microphone location. The two results for the overall sound pressure level (Figures 10(b) and 11) are almost identical. In particular, they both show that the cavity radiates as a dipole with the same intensities in the backward and forward directions. This is what one would expect at such low Mach numbers,[42] for which the convection of the acoustic emission by the flow over the cavity is negligible. In contrast, the overall sound pressure level computed with Curle's analogy without the image principle shows a strong emission directivity in the backward direction, although a dipolar behavior is still visible.

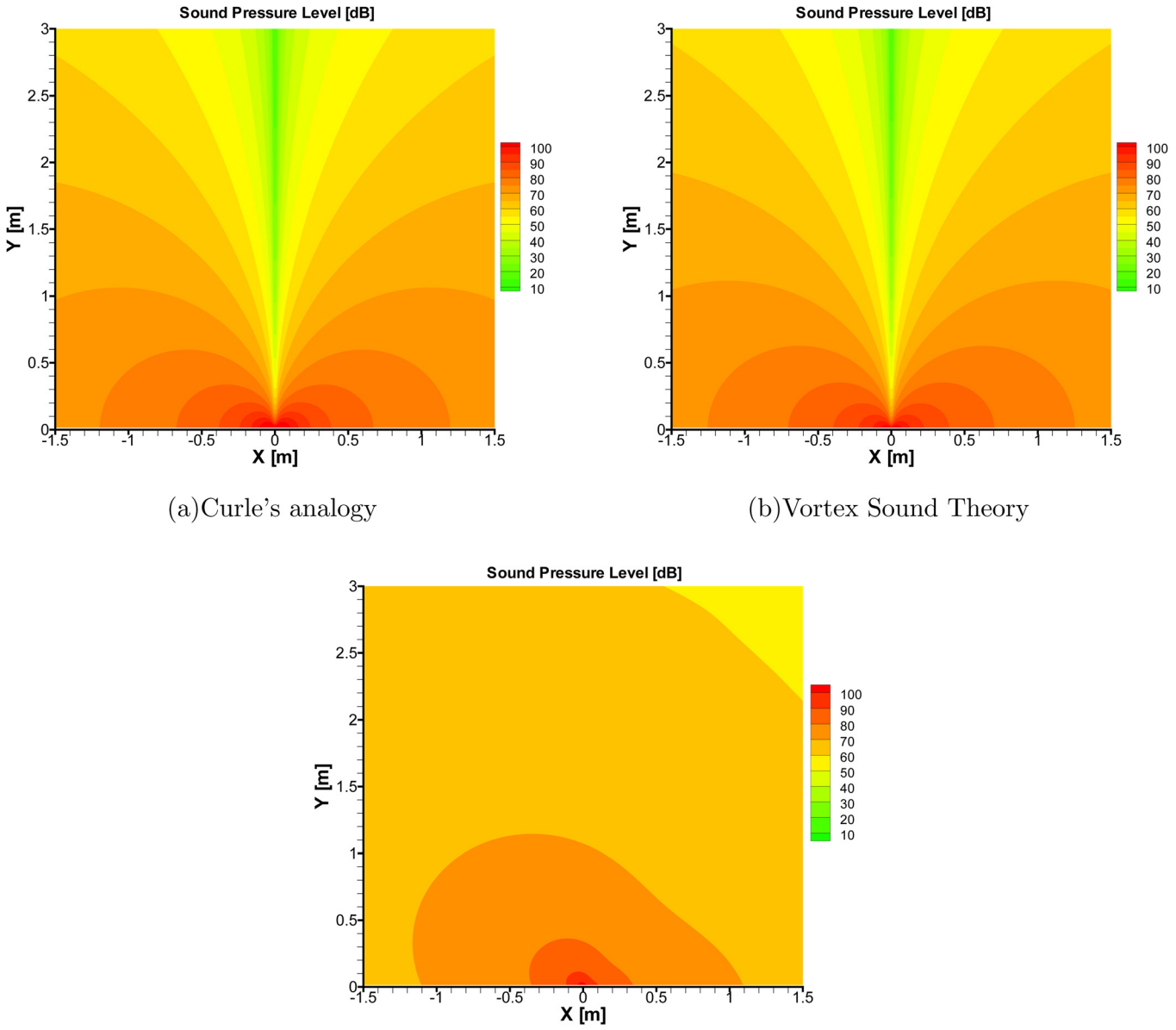

FIG. 11. (Color online) Computed overall sound pressure level, [dB], in the region above the cavity (the origin of the coordinates system is as shown in Figure 2).

IV. DISCUSSION AND CONCLUSIONS

In this paper, we compare two different acoustic analogies applied to time-resolved planar PIV data. The sound was computed using Curle's analogy and Vortex Sound Theory and compared with the directly measured acoustic data. The analogies used in this paper were derived under the assumption of low Mach number and high Reynolds number and for a listener positioned in the far field. We took into account the presence of the non-compact wall in which the cavity was located by using the image principle in the derivation of the solution. The two analogies give very similar results, both in total intensity and in the spectral distribution of the emitted sound. An analysis of the source terms for the two analogies reveals that the trailing edge of the cavity is the main source of sound in both cases. The fact that the quantitative results for the final solutions of the two methods are so similar, which provides confidence that they have been applied appropriately. The two solutions are in fact derived through quite different pathways, and the mathematical schemes used to solve the equations are sensitive to different factors. The analogies are therefore not interchangeable and which one performs better and is easier to apply depends on the specific application. Typically, the solution is affected by the temporal and the spatial resolution of the data, as well as by the noise level in the data. Those factors are always critical but affect the two analogies in different ways: for example, the temporal resolution has a stronger effect on the result obtained with Curle's analogy. Here, the source term is the pressure fluctuation at the walls that is approximated by the pressure fluctuation at the attainable position closest to the wall. The distance of this position from the wall

depends on the displacement of the flow during a time step and, therefore, is larger for large time steps in the PIV recording. On the other hand, the result obtained with the Vortex Sound Theory is heavily affected by noise in the data, as a matter of fact much more than Curle's analogy. The source term in the Vortex Sound Theory is the time derivative of the term $(\boldsymbol{\omega}\times\mathbf{u})\cdot\nabla Y_1$ (Eq. (17)). The vorticity $\boldsymbol{\omega}$ and the Lamb vector $\boldsymbol{\omega}\times\mathbf{u}$ are computed locally, and therefore if the data are noisy, the temporal derivation might be critical and leads to spurious high intensity source terms. This is especially a problem close to the sharp corners where the term Y_1 can attain very high values. In Curle's analogy, noisy data do not affect the final result very much. There, the source term is the pressure time derivative. The instantaneous pressure field is computed by integrating a Poisson equation over the whole domain and, therefore, the local error due to noise on every point is re-distributed over the entire domain. Another factor to take into consideration is the choice of the analogy is the complexity of the geometry. Vortex Sound Theory needs a Green's function tailored to the body geometry, which may not always be as straightforward to obtain as in the present geometry. In most cases, an analytical solution cannot be found and the Green's function has to be computed numerically, slightly increasing the complexity of the method.

In conclusion, both analogies perform quite well for the present test case, but in their application they show to have different strengths and weaknesses. The choice for either of the two methods needs to be done by carefully evaluating these aspects in relation to the specific application. The use of the image principle has been shown to be crucial to properly estimate the sound emission for compact geometries, sources of sound, which occur in large non-compact surfaces. The method applies to any compact geometry (such as cavities, projections, spoilers, etc.) that occur in a planar and extended surface[18,35] and for listeners positioned in the far field. The extension to more complex geometries is rather simple. For Curle's analogy, there is no additional complication, since the only geometry-related information in the solution is the wall normal direction, that is always easily available. For the Vortex Sound Theory, the numerical computation of the tailored Green's function may be necessary for those geometries for which an analytical solution is not known. This is usually not difficult, under the compactness and far-field assumptions, since it reduces to the simple computation of the flow potential over the geometry.

In the future, we plan to extend our research to the application of acoustic analogies to PIV experimental data on two main aspects: First, to perform a tomographic PIV study to evaluate the impact of neglecting terms in the sound prediction due to the fact that we base the computation on planar PIV measurements. Second, to evaluate, by means of numerical simulations, the effect of limited temporal and spatial resolution typical for the PIV data.

ACKNOWLEDGMENTS

This work is part of the research program of the Foundation for Fundamental Research on Matter (FOM), which is financially supported by the Netherlands Organization for Scientific Research (NWO).

[1]R. Dougherty, "Beam forming in Acoustic Testing," in *Aeroacoustic Measurements* (Springer, New York, 2002), pp. 62–97.
[2]T. F. Brooks and W. M. Humphreys, Jr., "A deconvolution approach for the mapping of acoustic sources (DAMAS) determined from phased microphone array," J. Sound Vib. **294**, 856 (2006).
[3]A. Henning, K. Kaepernick, K. Ehrenfried, L. Koop, and A. Dillmann, "Investigation of aeroacoustic noise generation by simultaneous particle image velocimetry and microphone measurements," Exp. Fluids **45**, 1073 (2008).
[4]A. Henning, L. Koop, and K. Ehrenfried, "Simultaneous particle image velocimetry and microphone array measurements on a rod-airfoil configuration," AIAA J. **48**, 2263 (2010).
[5]M. Wang, J. Freund, and S. Lele, "Computational prediction of flow-generated sound," Annu. Rev. Fluid Mech. **18**, 483 (2006).
[6]T. Colonius and S. Lele, "Computational aeroacoustics: Progress on nonlinear problems of sound generation," Prog. Aerosp. Sci. **40**, 345 (2004).
[7]T. Colonius, "Modeling artificial boundary conditions for compressible flow," Annu. Rev. Fluid Mech. **36**, 315 (2004).
[8]C. Schram, "Aeroacoustics of subsonic jets: Prediction of the sound produced by vortex pairing based on particle image velocimetry," Ph.D. thesis (Technische Universiteit Eindhoven, 2003).
[9]C. Haigermoser, "Application of an acoustic analogy to PIV data from rectangular cavity flows," Exp. Fluids **47**, 145 (2009).
[10]V. Koschatzky, P. D. Moore, J. Westerweel, F. Scarano, and B. J. Boersma, "High-speed PIV applied to aerodynamic noise investigation," Exp. Fluids **50**, 863 (2011).
[11]P. D. Moore, V. Lorenzoni, and F. Scarano, "Two techniques for PIV-based aeroacoustic prediction and their application to a rod-airfoil experiment," Exp. Fluids **50**, 877 (2011).
[12]V. Lorenzoni, D. Violato, and F. Scarano, "Characterization of the noise sources in a rod-airfoil configuration by means of time-resolved tomographic PIV," in Proceedings of the 16th AIAA/CEAS Aeroacoustics Conference, Melbourne (Australia), August 25–28, 2009.
[13]D. Violato, P. Moore, K. Bryon, and F. Scarano, "Application of Powell's analogy for the prediction of vortex-pairing sound in a low-Mach number jet based on time-resolved planar and tomographic PIV," in Proceedings of the 16th AIAA/CEAS Aeroacoustics Conference, Melbourne (Australia), August 25–28, 2009.
[14]P. Moore, D. Violato, K. Bryon, and F. Scarano, "On the suitability of direct application of acoustic theory to time-resolved tomographic PIV tested by DNS for low Mach number jet flows," in Proceedings of the 16th AIAA/CEAS Aeroacoustics Conference, Melbourne (Australia), August 25–28, 2009.
[15]V. Koschatzky, J. Westerweel, and B. Boersma, "Comparison of two acoustic analogies applied to experimental PIV data for cavity sound emission estimation," in Proceedings of the 16th AIAA/CEAS Aeroacoustics Conference, Melbourne (Australia), August 25–28, 2009.
[16]N. Curle, "The influence of solid boundaries upon aerodynamic sound," Proc. R. Soc. London, Ser. A **231**, 505 (1955).
[17]A. Powell, "Theory of vortex sound," J. Acoust. Soc. Am. **36**, 177 (1964).
[18]M. Howe, *Theory of Vortex Sound* (Cambridge University Press, New York, 2003).
[19]A cavity is called open when the ratio between its length and depth is larger than one.
[20]W. Rowley, T. Colonius, and A. Basu, "On self-sustained oscillations in two-dimensional compressible flow over rectangular cavities," J. Fluid Mech. **455**, 315 (2002).
[21]K. Ahuja and J. Mendoza, "Effects of cavity dimensions, boundary layer, and temperature on cavity noise with emphasis on benchmark data to validate computational aeroacoustic codes," NASA Report No. CR-4654, 1995.
[22]M. Gharib and A. Roshko, "The effect of flow oscillations on cavity drag," J. Fluid Mech. **177**, 501 (1987).
[23]J. E. Rossiter, "Wind tunnel experiments on the flow over rectangular cavities at subsonic and transonic speeds," ARC Reports and Memoranda 3438, 1964.
[24]M. Howe, "Edge, cavity and aperture tones at very low Mach numbers," J. Fluid Mech. **330**, 61 (1997).
[25]V. Suponitsky, E. Avital, and M. Gaster, "On three-dimensionality and control of incompressible cavity flow," Phys. Fluids **17**, 104103 (2005).

[26]C. K. W. Tam and P. J. W. Block, "On the tones and pressure oscillations induced by flow over rectangular cavities," J. Fluid Mech. **89**, 373 (1978).
[27]H. H. Heller and D. B. Bliss, "The physical mechanism of flow-induced pressure fluctuations in cavities and concepts for their suppression," AIAA Paper 1975–491, 1975.
[28]J. Westerweel, D. Dabiri, and M. Gharib, "The effect of a discrete window offset on the accuracy of cross-correlation analysis of PIV recordings," Exp. Fluids **23**, 20 (1997).
[29]F. Scarano, "Iterative image deformation methods in PIV," Meas. Sci. Technol. **13**, R1 (2002).
[30]X. Gloerfelt, C. Bailly, and D. Juvé, "Direct computation of the noise radiated by a subsonic cavity flow and application of integral methods," J. Sound Vib. **266**, 119 (2003).
[31]J. Larsson, L. Davidson, M. Olsson, and L. Eriksson, "Aeroacoustic investigation of an open cavity at low Mach number," AIAA J. **42**(12), 2462 (2004).
[32]M. Lighthill, "On sound generated aerodynamically. Part 1. General theory," Proc. R. Soc. London, Ser. A **211**, 564 (1952).
[33]A. Powell, "Aerodynamic noise and the plane boundary," J. Acoust. Soc. Am. **32**, 982 (1960).
[34]X. Liu and J. Katz, "Instantaneous pressure and material acceleration measurements using a four-exposure PIV system," Exp. Fluids **41**, 227 (2006).
[35]M. Howe, *Acoustics of Fluid-Structure Interactions* (Cambridge University Press, New York, 1998).
[36]V. Ivanov and M. Trubetskov, *Handbook of Conformal Mapping with Computer-aided Visualization* (CRC, Boca Raton, Florida, 1995).
[37]M. Abramowitz and I. Stegun, *Handbook of Mathematical Functions* (Dover Publications, New York, 1965).
[38]M. Raffel, C. Willert, S. Wereley, and J. Kompenhans, *Particle Image Velocimetry, a Practical Guide* (Springer, New York, 2007).
[39]J. Foucaut and M. Stanislas, "Some considerations on the accuracy and frequency response of some derivative filters applied to particle image velocimetry vector fields," Meas. Sci. Technol. **13**, 1058 (2002).
[40]J. Westerweel, "Digital particle image velocimetry: Theory and application," Ph.D. thesis (Delft University of Technology, 1993).
[41]P. Block, "Noise response of cavities of varying dimensions at subsonic speeds," NASA TN D-8351, 1976.
[42]M. S. Howe, "Mechanism of sound generation by low Mach number flow over a wall cavity," J. Sound Vib. **273**, 103 (2004).
[43]M. Priestley, *Spectral Analysis and Time Series* (Academic, London, 1981).
[44]Computed from the main tonal frequency: $\lambda = 0.6$ m.
[45]V. Sarohia, "Experimental and analytical investigation of oscillations in flows over cavities," Ph.D. thesis (California Institute of Technology, 1975).